Eur Phys J C **33**, s01, s149–s166 (2004)
Digital Object Identifier (DOI) 10.1140/epjcd/s2004-03-1751-x

EPJ C direct
electronic only

Review of astroparticle physics

Stefan Schael

I. Physikalisches Institut, RWTH Aachen, 52074 Aachen, Germany

Received: 9 January 2004 / Accepted: 16 February 2004 /
Published Online: 5 March 2004 –

Abstract. Observational cosmology is currently in its golden years. Using a variety of observational techniques the anisotropy of the CMB and the large-scale structure of the Universe is explored. In combination with large statistics observations of Supernova Ia and the measurement of the Hubble parameter by the HST key project cosmological parameters such as the total density of the universe and the rate of cosmological expansion are being precisely measured for the first time. A consistent standard picture of the universe is beginning to emerge. Recent developments in cosmology show that the interplay between astrophysics and particle accelerator results will allow us to perform tests of fundamental theories which cannot be done by accelerator experiments alone. A new generation of space experiments for the precision measurements of cosmic rays like PAMELA, GLAST and AMS will open a new window to understand the nature of dark matter. DAMA has claimed evidence with 6.3 σ C.L. to have observed the expected annual modulation for a WIMP signal. A variety of direct WIMP search experiments have shown evidence that they will reach within the next few years a sensitivity necessary to discover dark matter as predicted by SUSY models.

1 The standard model of cosmology

The "Standard Model of Cosmology" (SMC) [1] is based on the "cosmological principle": the Universe is isotropic and homogeneous on large scales. The cosmos, viewed from any point, looks the same as when viewed from any other point.

To express the cosmological principle mathematically, as a symmetry, one needs to define a metric. The most general line element consistent with homogeneity and isotropy is

$$ds^2 = dt^2 - a^2(t)d\mathbf{x}^2 \tag{1}$$

where the scale factor $a(t)$ contains all the dynamics of the universe, and the vector product $d\mathbf{x}^2$ contains the geometry of the space, which can be either Euclidean ($d\mathbf{x}^2 = dx^2 + dy^2 + dz^2$) or positively or negatively curved. In this Friedmann- Robertson-Walker (FRW) space, spatial distances are multiplied by a dynamical factor $a(t)$ that describes the expansion (or contraction) of the space time.

Einstein's field equations

$$G_{\mu\nu} = 8\pi G T_{\mu\nu} \tag{2}$$

where $G_{\mu\nu}$ is the Einstein Tensor, $T_{\mu\nu}$ is a stress energy tensor describing the distribution of mass in space and G is Newton's gravitational constant, take a particularly simple form, with the general metric from 1:

$$\left(\frac{\dot{a}}{a}\right)^2 = \frac{8\pi G}{3}\rho - \frac{k}{a^2} \tag{3}$$

with $k = -1, 0, +1$ depending on whether the curvature of the Universe is positive, zero or negative, respectively. Here ρ is the total energy density of the Universe. In addition, we have a second-order equation

$$\frac{\ddot{a}}{a} = \frac{4\pi G}{3}(\rho + 3p) \tag{4}$$

The second derivative of the scale factor depends on the equation of state of the fluid which is given by the parameter w, or $p = w\rho$. For any fluid with positive pressure, $w > 0$, the expansion of the universe is gradually decelerating, $\ddot{a} < 0$: the mutual gravitational attraction of the matter in the universe slows the expansion down.

In this uniformly expanding Universe Hubble's law is valid

$$v = H \cdot d \tag{5}$$

with the Hubble parameter

$$H(t) = \frac{\dot{a}(t)}{a(t)} \tag{6}$$

The Hubble parameter $H_0 \equiv H(t_0)$ at the present cosmic time t_0 will be called in the following the Hubble constant:

$$H_0 = h \cdot 100\ km/s/Mpc \tag{7}$$

Present observations give $h = 0.73 \pm 0.05$ [2].

The energy density of the Universe ρ has two contributions:

– ρ_m: The matter density which is the sum of radiation, baryonic matter and dark matter.

– $\rho_\Lambda = \Lambda/8\pi G$: The vacuum energy density, also called dark energy determined by the value of the cosmological constant Λ.

Define the critical density ρ_{crit} of the Universe by

$$\rho_c \equiv \frac{3H^2}{8\pi G} \tag{8}$$

and use 6 one can write 3 in the form

$$1 = \frac{\rho_{tot}}{\rho_{crit}} - \frac{k}{a^2H^2} \tag{9}$$

The present value of the critical energy density is

$$\rho_c^0 \equiv \frac{3H_0^2}{8\pi G} \approx 5 protons/m^3 \tag{10}$$

The overall geometry of the Universe is determined by the dimensionless parameter $\Omega_{tot} \equiv \rho_{tot}/\rho_{crit}$:

$$\frac{k}{a^2H^2} = \Omega_{tot} - 1 \tag{11}$$

If $\Omega_{tot} > 1$, k is positive, which means the Universe is closed and $a(t)$ can be chosen as the physical radius of the Universe which is still without boundary. If $\Omega_{tot} < 1$, the Universe has constant negative curvature and is open and could be of infinite extent. The limiting case $\Omega_{tot} \equiv 1$ would mean that the Universe is flat on large scales. It is important to note that Ω_{tot} in general depends on time.

In the following constraints on so called ΛCDM models that have no spatial curvature ($k = 0$) negligible neutrino masses $\Omega_\nu/\Omega_M = 0$ and dark energy corresponding to a pure cosmological constant ($w = -1$) will be discussed. These ΛCDM models are thus determined by six parameters: the matter budget (Ω_Λ, Ω_M, Ω_b) the initial conditions (A, n) (see 12) and the reionization optical depth τ.

According to all our present experimental data interpreted in the framework of the SMC the Universe is:

– spatially flat, homogeneous and isotropic on large scales
– composed of
  – 4.4% radiation, ordinary matter (electrons, protons, neutrons and neutrinos)
  – 23% cold dark matter
  – 73% dark energy.
– Galaxies and large scale structures grew gravitationally from tiny, nearly scale-invariant adiabatic Gaussian fluctuations.

Unfortunately none of the basic ingredients of this description of the Universe can be understood in the framework of the Standard Model of particle physics. We have no idea of the origin of the matter - anti-matter asymmetry which is the source of baryonic matter, we don't know anything about the nature of dark matter or dark energy and we have no theory to calculate the spectrum of quantum fluctuations in the early Universe.

As will be discussed in more detail in the following all present data sets from the various experiments on the cosmic microwave background, on large scale structure formation, on big bang nucleosynthesis and on supernova Ia which lead to a consistent description of the Universe when combined, need important priors to determine the relevant parameters of the SMC with interesting precision from their data alone. This is specially unsatisfactory as the underlying physics basis of the SMC is not understood. What is the nature of dark energy and dark matter ?

Only from the combination of astroparticle physics experiments with particle physics experiments we can expect to improve this situation in the near future. Specially for the important question about the nature of dark matter we can expect fresh inputs from the SUSY search at LHC, from the precision measurements of the anti-proton, the positron and gamma spectrum in cosmic rays by PAMELA, AMS and GLAST and from the direct WIMP search experiments which will reach a very interesting sensitivity in the coming years.

2 Cosmic microwave background

The measurements of the background of relic photons in the Universe, or cosmic microwave background [3], discovered by Penzias and Wilson at Bell Labs in 1963 are the key inputs today to determine the parameters of the SMC. The involved experiments have been a tremendous success and have changed our understanding of the Universe significantly.

The microwave background radiation is extremely uniform, varying in temperature by only a few parts in 10^5 [5] over the sky; its departure from a perfect blackbody spectrum has yet to be detected. The very existence of the microwave background provides crucial support for the Hot Big Bang cosmological model: the universe began in a very hot, dense state from which it expanded and cooled.

Quantum fluctuations in the early universe lead to density fluctuations at the time of recombination[1] (t_R). These nearly scale-invariant adiabatic Gaussian fluctuations are described by a power spectrum

$$P(k) = A \cdot k^n \tag{12}$$

with $k = 2\pi/\lambda$. The amplitude A and the spectral index n are free parameters in the SMC and have to be determined from experimental data.

[1] This epoch is erroneously referred to as "recombination", despite the fact that electrons and nuclei had never before "combined" into atoms.

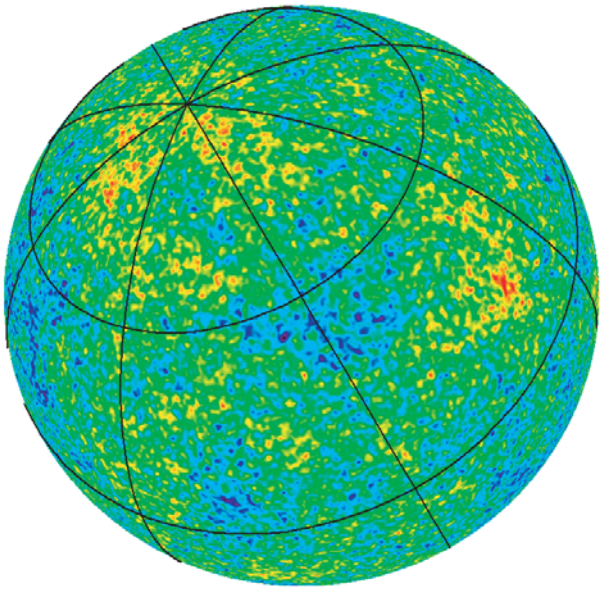

Fig. 1. The surface of last scatter appears to every observer as a sphere centered around himself. From [3]

At a redshift z of:

$$1 + z = \frac{a(t_0)}{a(t_R)} = \frac{T_R}{T_0} \approx \frac{3000\ K}{2.73\ K} \approx 1100 \qquad (13)$$

the surface of last scattering appears to us as a spherical surface (see Fig. 1).

Therefore the natural parameterization is an expansion of the CMB sky in spherical harmonics:

$$\frac{T(\hat{n})}{T_0} = 1 + \sum_{l=1}^{\infty} \sum_{m=-l}^{l} a_{lm}^T Y_{lm}(\hat{n}) \qquad (14)$$

where

$$a_{lm}^T = \frac{1}{T_0} \int d\hat{n} T(\hat{n}) Y_{lm}^*(\hat{n}) \qquad (15)$$

The a_{lm} are the expansion coefficients like the individual amplitudes in a Fourier series.

The T angular power spectrum is then given by

$$C_l^{TT} \delta_{ll'} \delta mm' \equiv \left\langle a_{lm}^{T*} a_{l'm'}^T \right\rangle \qquad (16)$$

The angled brackets represent an average over statistical realizations of the underlying distribution. Since there is no preferred direction in the universe, the physics is independent of the index m, and we can define as an unbiased estimator:

$$\hat{C}_l^{\ TT} \equiv \frac{1}{2l+1} \sum_m a_{lm}^{T*} a_{lm}^T \qquad (17)$$

The statistical uncertainty

$$\Delta C_l^{TT} = \sqrt{\frac{2}{2l+1}} C_l^{TT} \qquad (18)$$

is known as the "cosmic variance".

The dominant processes which are responsible for temperature fluctuations in the CMB are acoustic oscillations in the baryon/photon plasma. Compressing a gas heats it up. Letting it expand cools it down. The CMB is locally hotter in regions where the acoustic wave causes compression and cooler where it causes rarefaction.

The position of the bumps in l is determined by the oscillation frequency of the mode. The first bump is created by modes that have had time to go through half an oscillation in the age of the universe (compression). The second bump is created by modes that have gone through one full oscillation (rarefaction) and so on.

The sensitivity of the angular power spectrum to the total energy density Ω_{tot}, to the baryon density $\Omega_b h^2$ and to the total matter density $\Omega_m h^2$ can be seen in Fig. 2 [3]:

- decreasing Ω_{tot} from 1 moves the curve to the right
- varying Ω_Λ while keeping $\Omega_{tot} = 1$ fixed has nearly no effect at larger values of l.
- decreasing $\Omega_b h^2$ decreases the height of the first peak while increasing the height of the second peak
- decreasing $\Omega_m h^2$ moves the whole spectrum up and to larger l.

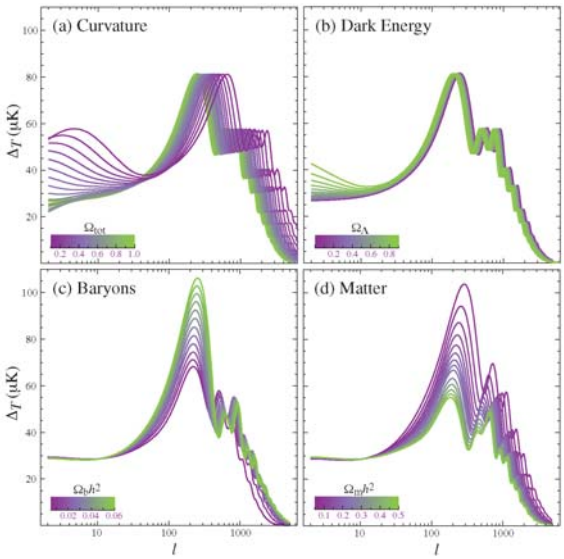

Fig. 2. The sensitivity of the angular power spectrum to Ω_{tot} (a), Ω_Λ (b), $\Omega_b h^2$ (c) and $\Omega_m h^2$. While varying one parameter the others are fixed at $\Omega_{tot} = 1.0$, $\Omega_\Lambda = 0.65$, $\Omega_b h^2 = 0.02$, $\Omega_m h^2 = 0.147$. From [3]

2.1 CMB – polarization

From Thomson scattering one expects that up to 10% of the anisotropies at a given scale are polarized. Polarization fluctuations reflect mainly velocity perturbations at last scattering, in contrast to temperature fluctuations which predominantly reflect density perturbations [3].

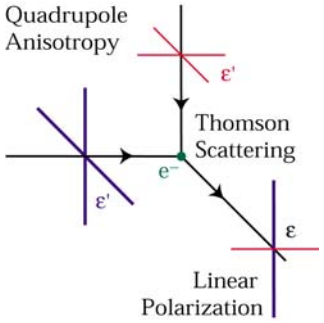

Fig. 3. CMB Polarization by Thomson scattering

The Thomson scattering cross section depends on the polarization:

$$\frac{d\sigma_T}{d\Omega}(e^{\pm} + \gamma \to e^{\pm}\gamma) \propto |\hat{\epsilon} \cdot \hat{\epsilon}'|^2 \tag{19}$$

If the incoming radiation field is isotropic one gets no polarization, but if the incoming radiation field possesses a quadrupolar variation in intensity or temperature, the result is a linear polarization of the scattered radiation.

The polarization field can be analyzed in a way similar to the temperature field. The complication is, that in addition to its strength polarization has an orientation, depending on the relative strength of the two linear polarization states. Classically polarization is described in terms of the Stokes parameters Q and U. A monochromatic wave propagating in the z-direction has the electrical field vector

$$E_{x,y} = a_{x,y}(t)\cos[\omega_0 t - \Theta_{x,y}(t)] \tag{20}$$

The Stokes parameters are defined as the following time averages

$$I \equiv < a_x^2 > + < a_y^2 > \tag{21}$$
$$Q \equiv < a_x^2 > - < a_y^2 > \tag{22}$$
$$U \equiv < 2a_x a_y cos(\Theta_x - \Theta_y) > \tag{23}$$
$$V \equiv < 2a_x a_y sin(\Theta_x - \Theta_y) > \tag{24}$$

The intensity of the radiation is given by I which is always positive and is equivalent to the temperature for blackbody radiation. The other three parameters define the polarization state of the wave and can have either sign. Unpolarized radiation, or "natural light", is described by $Q = U = V = 0$. Thomson scattering can give no net circular polarization, so $V = 0$ for cosmological perturbations.

Cosmologists prefer the scalar E and the pseudo-scalar B, linear combinations of Q and U. In complete analogy to the decomposition of the temperature fluctuations in terms of multipol moments one gets the following power spectra [3]:

$$C_l^{TT},\ C_l^{EE},\ C_l^{TE},\ C_l^{BB} \tag{25}$$

Polarization measurements allow to test the priors which are used to analyze CMB data like the reionization optical depth τ or the redshift at which the Universe was re-ionized $7 < z_i < 20$. The EE-polarization is down by a factor of 10 in temperature and anti-correlated to T-fluctuations. The BB-polarization is even smaller and can not be produced by density perturbations but only by gravitational waves.

2.2 The WMAP experiment

There are at present about thirty experiments (in satellites, from the ground and balloon-borne) looking at the microwave background temperature anisotropies with angular resolutions from 7° to a few arc minutes in the sky, corresponding to multipol numbers $l = 2-3000$. The most relevant experimental data on the CMB angular power spectrum are summarized in Fig. 4. The new results from the Wilkinson Microwave Anisotropy Probe (WMAP) [6] dominate the measurements at low l and will be discussed in more detail in the following.

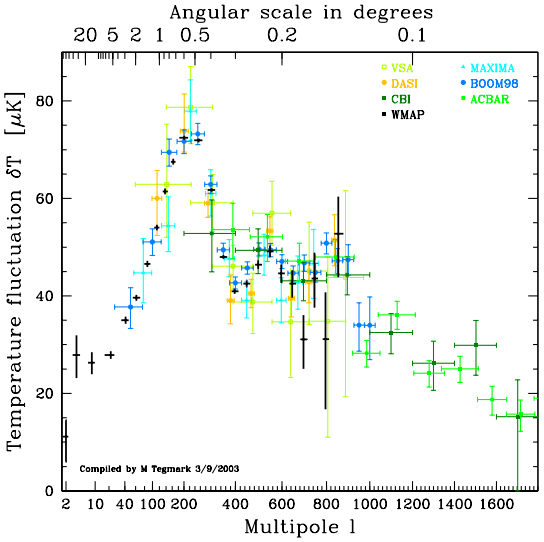

Fig. 4. Experimental data on the CMB angular power spectrum taken from [4]

The WMAP experiment [6] if shown on Fig. 5. The WMAP Instrument design philosophy was driven by the idea to control systematic effects by designing for extreme stability (temperature, voltage, enviroment). For the experiment a design with differential radiometers, passive cooling and a complex scan pattern was chosen. The orbit at Earth-Sun L2 Lagrange point eliminates the two largest contributions to the systematic errors of COBE data: the Earth's magnetic field and the thermal emission from the Earth's limb. The design goal of $4\mu K$ limit on systematic

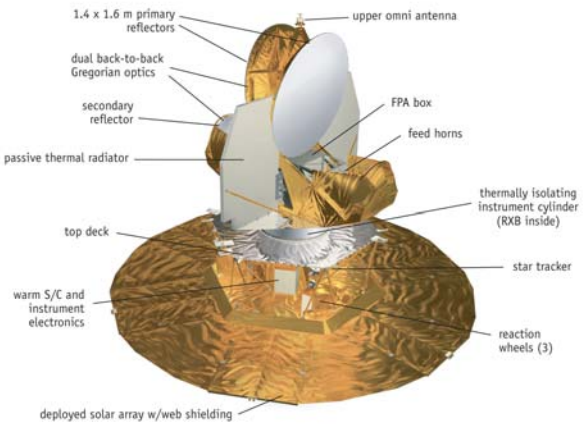

Fig. 5. The WMAP Experiment

errors was reached. No systematic corrections were needed in the data analysis. The final CMB map obtained from the WMAP experiment is shown in Fig. 6.

A comparison between the CMB maps obtained from COBE and WMAP is shown in Fig. 6. The angular resolution has been improved from 7° to 0.2° and the sensitivity by a factor 45.

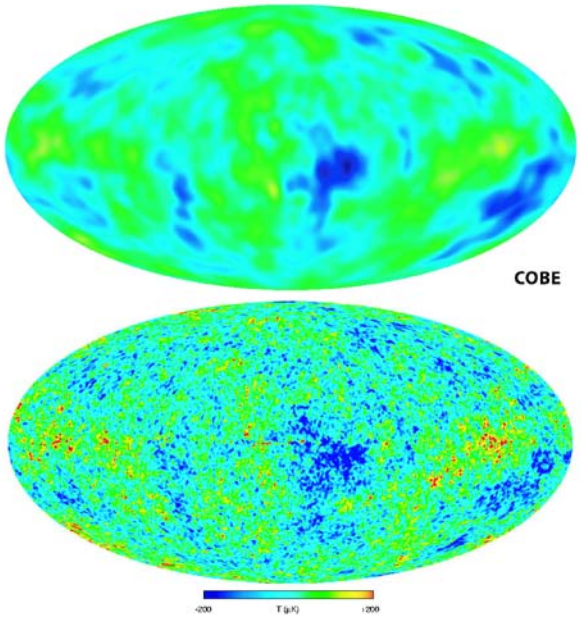

Fig. 6. Comparison of the CMB maps obtained from COBE (tob) and WMAP (*bottom*)

The WMAP angular power spectrum (see Fig. 7) is cosmic variance limited for $l < 354$ with a signal-to-noise ratio > 1 per mode to $l = 658$. As WMAP dominates the CMB measurements at low l in the following only the WMAP [7,8], the CBI [9] and the ACBAR [10] data

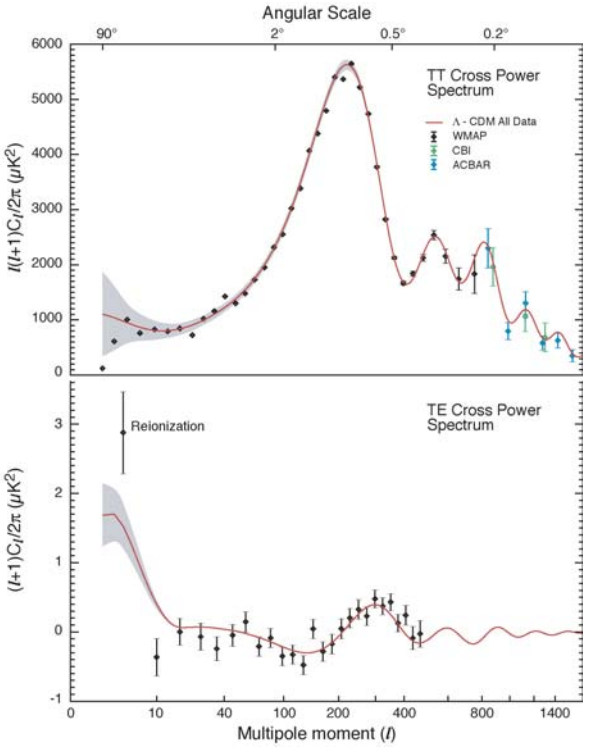

Fig. 7. The WMAP angular power spectrum. (top:) The WMAP temperature (TT) results are consistent with the ACBAR and CBI measurements, as shown. The best fit running index ΛCDM model is shown. The grey band represents the cosmic variance expected for that model. (bottom:) The temperature-polarization (TE) cross-power spectrum, $(l+1)C_l/2\pi$. The peak in the TE spectrum near $l \approx 300$ is out of phase with the TT power spectrum, as predicted for adiabatic initial conditions. The anti-peak in the TE spectrum near $l \approx 150$ is evidence for super-horizon modes at decoupling, as predicted by inflationary models. From [7]

are used to determine the parameters of the SMC. The parameters of the SMC as determined from these measurements are summarized in Table 1. The value of the Hubble constant is in excellent agreement with the value of $h = 0.72 \pm 0.3 \pm 0.7$ as measured by the HST Key Project [11] with the Hubble space telescope.

To obtain these results from the WMAP, CBI and ACBAR data the important prior $\Omega_{tot} = 1.0$ has been used. Only the combination of WMAP data with either H_0, Type Ia SNe, or large scale structure data constrains $|1 - \Omega_{tot}| < 0.03$ [2].

The WMAP data test several of the key tenets of the SMC. The WMAP data alone enable accurate determinations of many of the key cosmological parameters. The obtained results are consistent with the Big Bang theory and inflation. WMAP continues to collect data and is currently approved for 4 years of operations. The additional data, and more elaborate analyses, will help to further constrain models.

Table 1. The parameters of the SMC as determined from WMAP (first column) and in combination with the results from CBI [9] and ACBAR [10]. From [2]

	WMAP	WMAPext
A	0.9 ± 0.1	0.8 ± 0.1
n	0.99 ± 0.04	0.97 ± 0.03
τ	$0.166\ ^{+0.076}_{-0.071}$	$0.143 \pm\ ^{+0.071}_{-0.062}$
h	0.72 ± 0.05	0.73 ± 0.05
$\Omega_m h^2$	0.14 ± 0.02	0.13 ± 0.01
$\Omega_b h^2$	0.024 ± 0.001	0.023 ± 0.001
$\chi^2_{eff}/Ndof$	1429/1341	1440/1352

3 Structure formation

Large scale structure data sets are a powerful tool for breaking many of the parameter degeneracies associated with CMB data. The large scale structure observations and the Lyman α forest data complement the CMB measurements by measuring similar physical scales at very different epochs.

Cosmic inhomogeneities are described by

$$\delta(\mathbf{x}) = \frac{\rho(\mathbf{x}) - \bar{\rho}}{\bar{\rho}} \tag{26}$$

where $\rho(x)$ is the density of the Universe at the point x. A statistical characterization of the inhomogeneities in the distribution of cosmic structure is provided by the two-point correlation function, $\xi(r)$, which describes the expected excess fluctuations with respect to a uniform distribution:

$$\xi(r) =< \delta(\mathbf{x})\delta(\mathbf{x}+\mathbf{r}) > \tag{27}$$

where the symbol <> indicates the average over all the pairs of points with separation r. Its Fourier transform is the power spectrum

$$P(k) = \frac{1}{2\pi^2}\int_0^\infty dr\xi(r)\frac{\sin kr}{kr} \tag{28}$$

It is commonly assumed that $P(k)$ follows a simple power spectrum

$$P(k) = A \cdot k^n \tag{29}$$

where A is the amplitude and the spectral index n is close to 1.

3.1 The 2dF galaxy redshift survey

The 2dFGRS [14] was designed to study the large-scale structure in the galaxy distribution to measure the galaxy power spectrum $P(k)$ on scales up to a few hundred Mpc, bridging the gap between the scales of nonlinear structure and measurements from the cosmic microwave background.

Three dimensional distances are estimated using Hubble's law (6) of recessional velocity in an expanding Universe. The redshift z, is approximately the velocity v divided by the speed of light. This gives an estimate of the distance of the galaxies. These distances are plotted in Fig. 8 for a thin strip (4 degrees wide) of the survey galaxies.

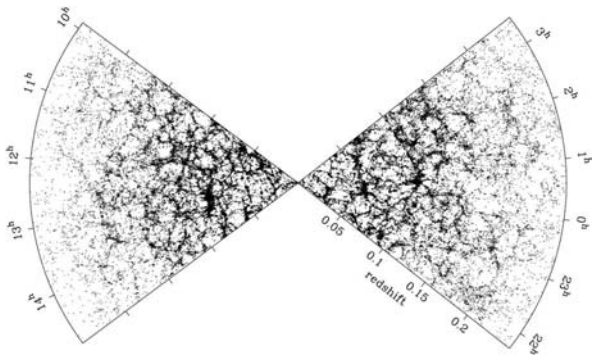

Fig. 8. This picture shows the distribution of approximately 63000 galaxies from the 2dF galaxy redshift survey

The 2dFGRS uses the 2dF spectrograph, which sits at the prime focus on the 3.9 m Anglo-Australian Telescope. The 2dF instrument uses fiber-optics to obtain the spectra of the up to 400 objects simultaneously over a 2 degree diameter field of view (see http://www.aao.gov.au/2df). Using a robotic positioner the instrument can take up to 400 redshifts an hour with no dead time.

The data (see Fig. 9) allow to infer that the baryonic matter density in the Universe is $\Omega_b = 0.044 \pm 0.016$ while the rest is dark matter. The total amount of matter is well constrained at $\Omega_m = 0.26 \pm 0.05$ assuming a Hubble constant of $h = 0.70 \pm 0.07$ and a value of the spectral index of the power spectrum of $n = 1$.

It is especially interesting to see that the combination of 2dFGRS data and CMB data allows to distinguish between cosmological models. To illustrate this point, the following three models are considered , all with $\Omega_\mathrm{b} = 0.024$:

1. A Mixed Dark Matter (MDM) model with $\Omega_M = 1$, $\Omega_\nu = 0.2$, $h = 0.45$, and $n = 0.95$.
2. A ΛCDM model with $\Omega_M = 0.3$, $\Omega_\nu = 0$, $h = 0.7$, and $n = 1.0$.
3. A pure CDM model with $\Omega_M = 1$, $\Omega_\nu = 0$, $h = 0.45$, and $n = 0.95$.

While one can clearly exclude the CDM-model from the 2dFGRS data this would not be possible from the CMB data alone without any input on the Hubble constant (see Fig. 9). But one could fit reasonable well both data sets with the Mixed Dark Matter Model if one allows low values for the Hubble constant $H_0 < 50\ km/s/Mpc$. This clearly shows the importance of priors in the interpretation of these data sets [15].

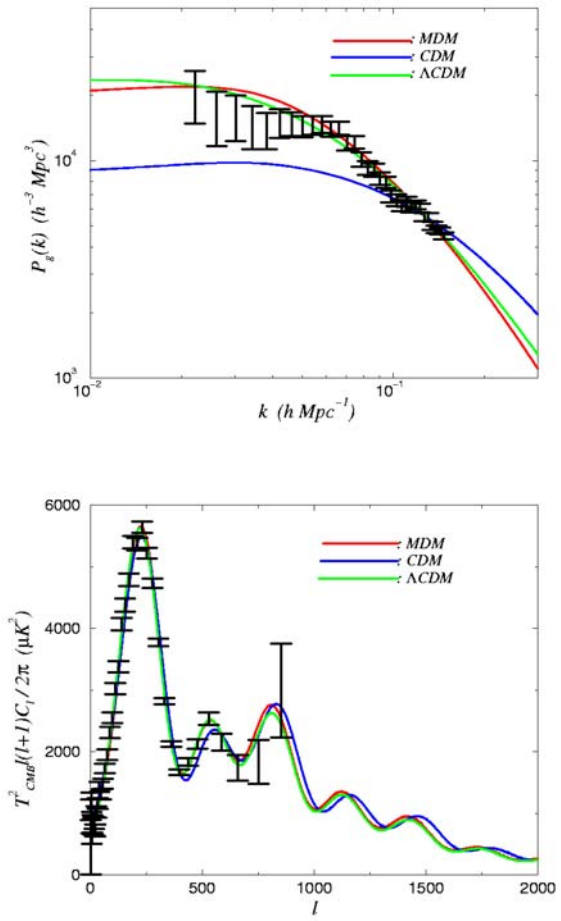

Fig. 9. Galaxy power spectrum as measured from the 2dFGRS (*top*) and Angular power spectrum of the CMB as measured from WMAP (*bottom*) compared to the MDM-, CDM- and the ΛCDM-model [15]

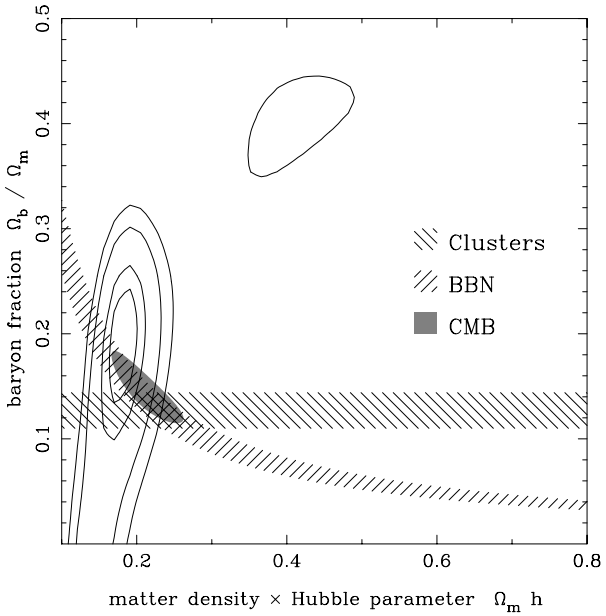

Fig. 10. Likelihood contours from the 2dFGRS compared to constraints from X-ray cluster analysis, big-bang nucleosynthesis and anisotropies in the CMB

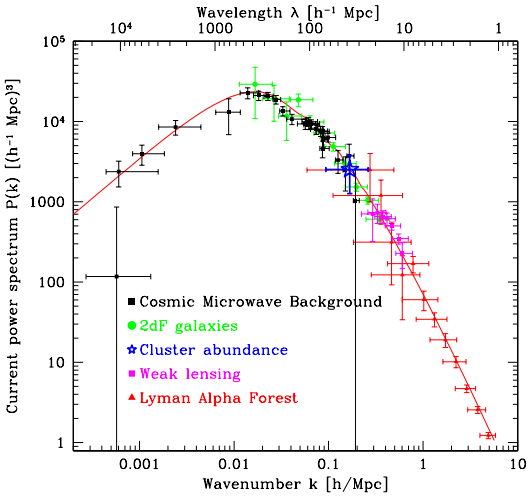

Fig. 11. Comparison of the 2dFGRS result with other P(k) constraints. The location of CMB, cluster, lensing and Lya forest points in this plane depends on the cosmic matter budget (and, for the CMB, on the reionization optical depth τ), so requiring consistency with 2dFGRS constrains these cosmological parameters without assumptions about the primordial power spectrum. From [4]

In Fig. 10 the 2dFGRS result is displayed together with constraints from X-ray cluster analysis, big-bang nucleosynthesis and anisotropies in the CMB.

The experimental data on the power spectrum are combined in Fig. 11. The various data sets agree very well and can be described in the so called "concordance" model with the following parameters of the SMC: A flat scalar scale-invariant model with $\Omega_m = 0.28$, $h = 0.72$, and $\Omega_b/\Omega_m = 0.16$, $\tau = 0.17$ [2,8,18].

3.2 Neutrino masses

The relic abundance of neutrinos in the Universe today can be derived from the fact that they continue to follow the Fermi-Dirac distribution after freeze- out, and their temperature is given in terms of the CMB temperature T_{CMB} today as $T_\nu = (4/11)^{1/3} T_{CMB}$,

$$n_\nu = N_\nu \frac{6\zeta(3)}{11\pi^2} \cdot \left(\frac{k_B T_{CMB}}{\hbar c}\right)^3 \qquad (30)$$

where $\zeta(3) \approx 1.202$, which gives $n_\nu \approx 336\ cm^{-3}$ at present for 3 neutrino flavours. Neutrinos are so light that they were ultra-relativistic at freeze-out. Their present contribution to the mass density can therefore be found by multiplying n_ν with the total mass of the neutrinos $m_\nu^{tot} = \sum m_i$, giving

$$\Omega_\nu h^2 = \frac{m_\nu^{tot}}{94\ eV} \tag{31}$$

for $T_{CMB} = 2.728\ K$.

Neutrinos affect structure formation because they are a source of Dark Matter. Different to Cold Dark Matter they are still relativistic when they drop out of thermal equilibrium, i.e when their interaction rate falls below the expansion rate of the Universe. Neutrinos can free-stream over large distances and erase small scale structure. Fluctuations are suppressed at wavenumbers

$$k = 0.026\sqrt{\frac{m_\nu}{1\ eV}}\Omega_m^{1/2} Mpc^{-1} \tag{32}$$

Clearly the inference of the neutrino mass depends on our assumptions ("priors") on the other parameters [15]. Using $\Omega_m h^2 = 0.15$ and $n = 1.0 \pm 0.1$ one gets from the 2dFGRS data [16] (see Fig. 12) an upper limit for the sum of the neutrino mass matrix eigenvalues $m_\nu^{tot} < 2.2\ eV$ @95% CL, i.e. approximately $m_\nu \approx 0.7\ eV$ for each neutrino flavour. It is very important to note, that this limit is very sensitive to the value of the Hubble constant which is taken from the HST key project [11].

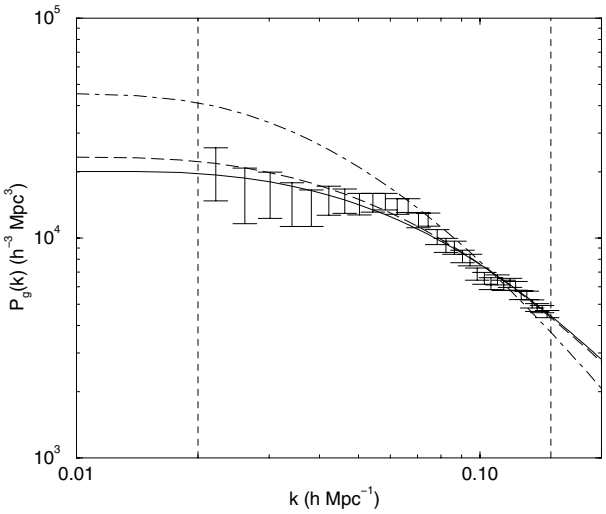

Fig. 12. Power spectra for $\Omega_\nu = 0$ (solid line), $\Omega_\nu = 0.01$ (dashed line), and $\Omega_\nu = 0.05$ (dot-dashed line) with amplitudes fitted to the 2dFGRS power spectrum data (vertical bars) in redshift space assuming $\Omega_m = 0.3$, $\Omega_\Lambda = 0.7$, $h = 0.7$ and $\Omega_b h^2 = 0.02$. The vertical dashed lines limit the range in k used in the fit

A combined analysis of the CMB, 2dFGRS and Ly-alpha data by the WMAP team leads to an improved limit for the neutrino mass of $m_\nu^{tot} < 0.7\ eV$ @95% CL [2].

In the near future we can expect significant improvement from the Sloan Digital Sky Survey (SDSS) [17] which uses a 2.5 m telescope in New Mexico (see www.sdss.org).

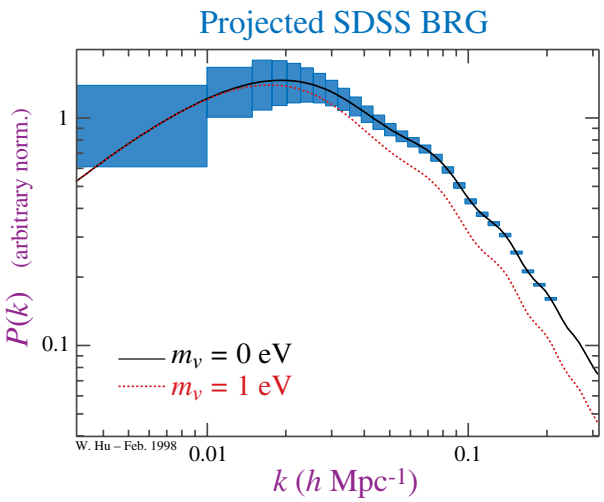

Fig. 13. Expected power spectrum from the SDDS together with the sensitivity to neutrino masses

This Sky Survey will systematically map one-quarter of the entire sky to determine the positions and absolute brightnesses of more than 100 million celestial objects. The expected improvement in the power spectrum is shown in Fig. 13 together with the sensitivity to the neutrino mass.

4 Big Bang Nucleosynthesis (BBN)

Both the amplitude of the acoustic peaks in the CMB spectrum and the primordial abundance of Deuterium are sensitive functions of the cosmological baryon density. The height and position of the acoustic peaks depend upon the properties of the cosmic plasma 372,000 years after the Big Bang and the Deuterium abundance depends on physics only three minutes after the Big Bang. Comparing the baryon density constraints inferred from these two different probes provides an important test of the Big Bang model.

The primordial light element abundances are predicted accurately and robustly by the theory of Big Bang Nucleosynthesis (BBN) [19], describing the first 3 minutes of the hot early universe.

In standard BBN, primordial abundances are sensitive to only one parameter, the baryon-to-photon ratio (see Fig. 14):

$$n_B/n_\gamma \equiv \eta \propto \Omega_b h^2 \tag{33}$$

The abundances of the light elements can be measured from:

- ^4He: extra-galactic HII regions, abundance by mass 25%
- ^7Li: atmospheres of dwarf halo stars, abundance by number 10^{-10}
- D: quasar absorption systems (and locally), abundance by number $3 \cdot 10^{-5}$

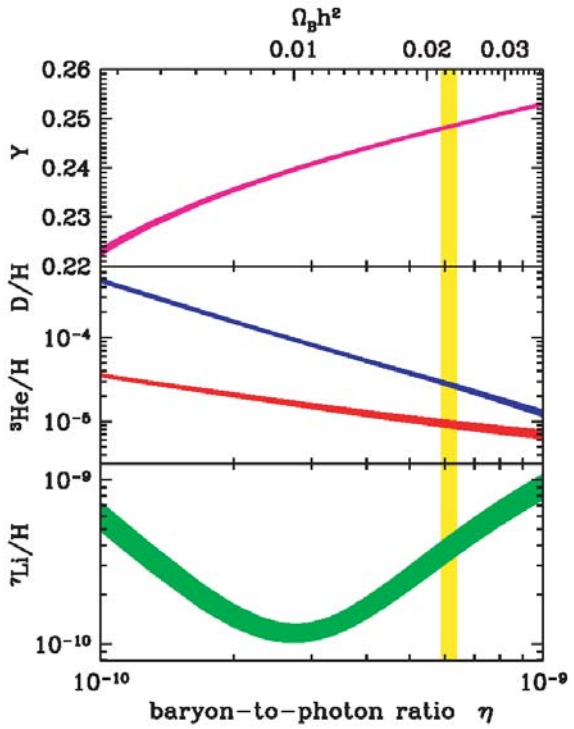

Fig. 14. Abundance predictions for standard BBN [21]; the width of the curves give the $1-\sigma$ error range. The WMAP η range (33) is shown in the vertical (yellow) band

– ^3He: solar wind, meteorites, and ISM, abundance by number 10^{-5}.

From the CMB data one finds for $\eta_{10} = \eta \cdot 10^{10}$:

$$\eta_{10} = 6.14 \pm 0.25 \Leftrightarrow \Omega_b h^2 = 0.0224 \pm 0.0009 \qquad (34)$$

while one gets from the BBN data:

$$\eta_{10} = 6.14 \, ^{+0.7}_{-0.5} \Leftrightarrow \Omega_b h^2 = 0.022 \, ^{+0.003}_{-0.002} \qquad (35)$$

in good agreement with the CMB data. It is impressive that the good understanding of the Universe at $z \approx 1100$ from the CMB data also confirms the understanding of the Universe at $z \approx 10^{10}$. This agreement gives great confidence in the soundness of the hot big bang cosmology.

5 Supernova Ia

Over the past decade, Type Ia supernova have been important cosmological probes. They are understood as a White Dwarf accreting material from a binary companion. As the White Dwarf reaches Chandrasekhar mass, a thermonuclear runaway is triggered. Supernovae Ia can therefore be considered as a natural triggered standard bomb.

Since the supernova data probes the luminosity distance versus redshift relationship at moderate redshift $z <$ 2 and the CMB data probes the angular diameter distance relationship to high redshift ($z \approx 1100$), the two data sets are complementary.

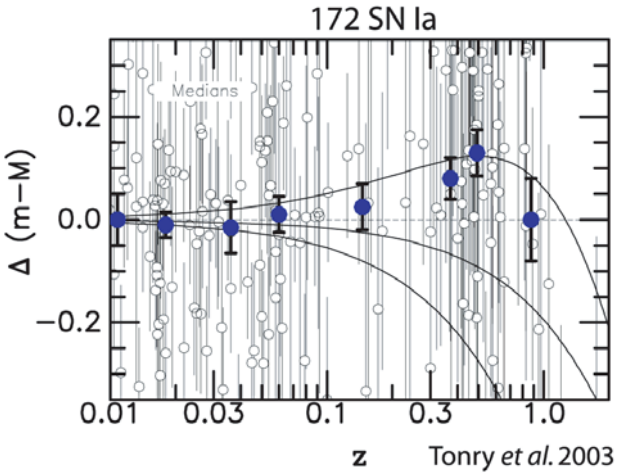

Fig. 15. The Fall 1999 and other data points are shown in a residual Hubble diagram with respect to an empty universe. In this plot the highlighted points correspond to median values in eight redshift bins. From top to bottom the curves show $(\Omega_M, \Omega_\Lambda) = (0.3, 0.7)$, (0.3,0.0), and (1.0,0.0), respectively

The High-z Supernova Search Team has observed 8 new supernovae [22] in the redshift interval $z = 0.3 - 1.2$. These independent observations confirm the result of Riess et al. (1998a) [23] and Perlmutter et al. (1999) [24] and imply an accelerating universe. More importantly, they extend the redshift range of consistently observed SN Ia to $z \approx 1$, where the signature of cosmological effects has the opposite sign of some plausible systematic effects. Consequently, these measurements not only provide another quantitative confirmation of the importance of dark energy, but also constitute a powerful qualitative test for the cosmological origin of cosmic acceleration.

In total the High-z Supernova Search Team presents data for 230 SN Ia (see Fig. 15) [22]. These place significant constraints on cosmological quantities if the equation of state parameter of the dark energy is $w = p/\rho = -1$ where p and ρ are pressure and density of the dark energy. A cosmological constant has $w = -1$. Including in addition the constraint of a flat Universe, one finds $\Omega_M = 0.28 \pm 0.05$ (see Fig. 16) [22], independent of any large-scale structure measurements.

Adopting a prior based on the 2dF redshift survey constraint on Ω_M and assuming a flat universe, we find that the equation of state parameter of the dark energy lies in the range $-1.48 < w < -0.72$ at 95% confidence (see Fig. 17 [22]). These constraints are similar in precision and in value to recent results reported using the WMAP satellite, also in combination with the 2dF redshift survey.

In the future significant improvements can be expected if SNAP (details at http://snap.lbl.gov) which is a a

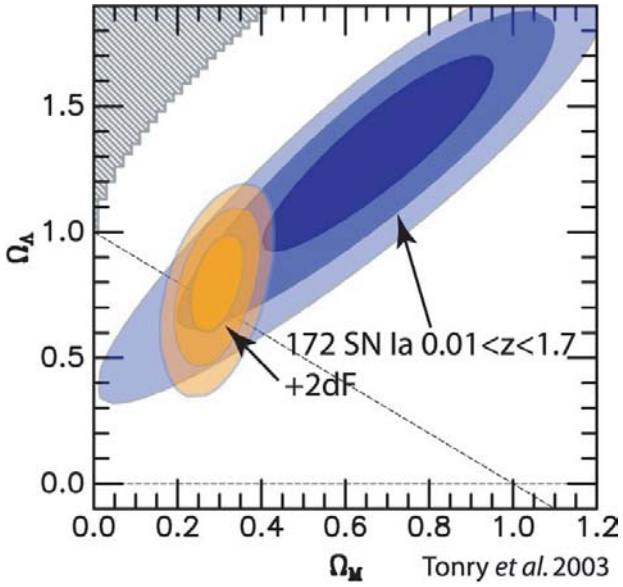

Fig. 16. Probability contours for Ω_Λ versus Ω_M are shown at 1σ, 2σ, and 3σ with $w = -1$. We also give 1σ, 2σ, and 3σ contours when we adopt a prior of $\Omega_M h = 0.20 \pm 0.03$ from the 2dF survey (Percival et al. 2001). These constraints use the full sample of 172 SN Ia with $z > 0.01$ and $A_V < 0.5mag$

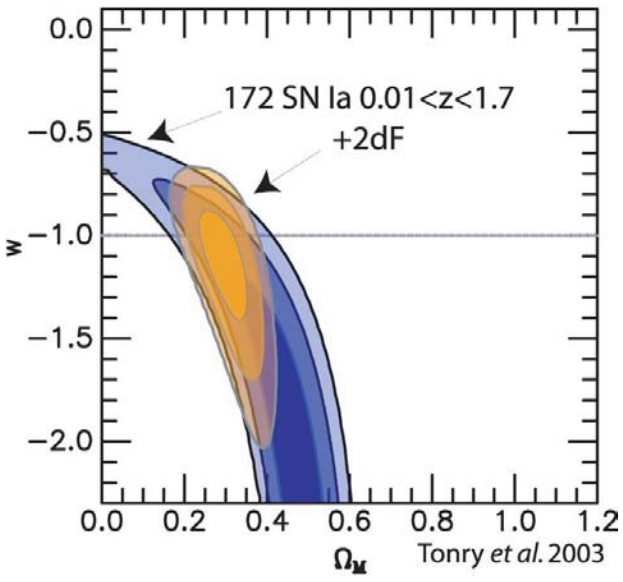

Fig. 17. Probability contours for dark energy parameter w versus Ω_M are shown at 1σ, 2σ, and 3σ when $\Omega_{tot} = 1$. We also give 1σ, 2σ, and 3σ contours when we adopt a prior of $\Omega_M h = 0.20 \pm 0.03$ from the 2dF survey (Percival et al. 2001). This sample includes all 172 SN Ia with $z > 0.01$ and $A_V < 0.5mag$

space-based optical/NIR survey telescope is realized (see Fig. 18). The SNAP satellite is a 2 m aperture telescope which should be able to measure 2000 supernovae per year with redshift of up to $z \approx 2$. From the decision it is expected to take 4 years to construct and launch the satellite.

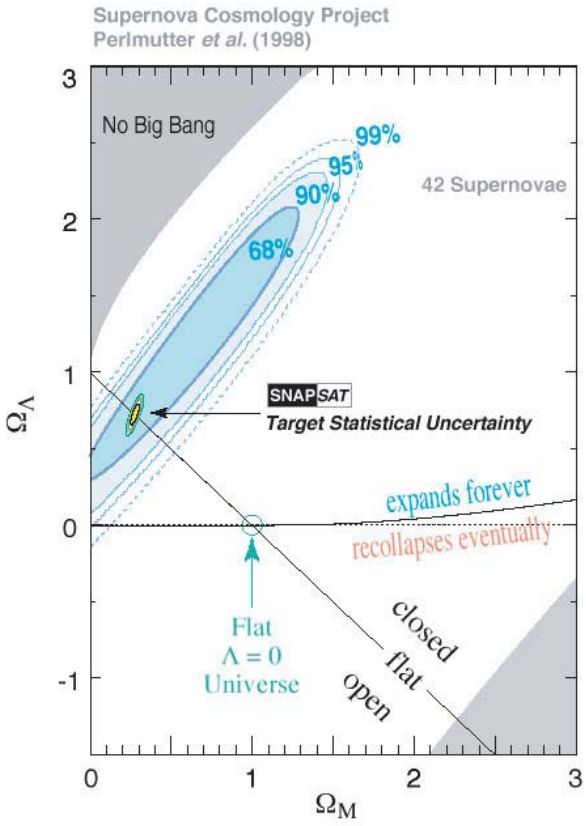

Fig. 18. Expected constraints in the $\Omega_\Lambda - \Omega_M$ plane from the SNAP satellite compared to other constraints from supernova measurements

Table 2. Best fit parameters: power law ΛCDM model from [2]

	WMAPext	WMAPext +2dFGRS + Lyman α
A	0.8 ± 0.1	$0.75^{+0.08}_{-0.07}$
n	0.97 ± 0.03	0.96 ± 0.02
τ	$0.143 \pm ^{+0.071}_{-0.062}$	$0.117^{+0.057}_{-0.053}$
h	0.73 ± 0.05	0.72 ± 0.03
$\Omega_m h^2$	0.13 ± 0.01	0.133 ± 0.006
$\Omega_b h^2$	0.023 ± 0.001	0.0226 ± 0.0008

6 Combination of observables

The cosmological parameters describing the best fit power law ΛCDM model are summarized in Table 2 and displayed in Fig. 19 [2].

7 Search for cold dark matter

The combination of the various cosmological observations presents strong evidence for the existence of cold dark matter. Further evidence is provided by gravitational lensing measurements and by the measurements of rotational curves of nearby galaxies.

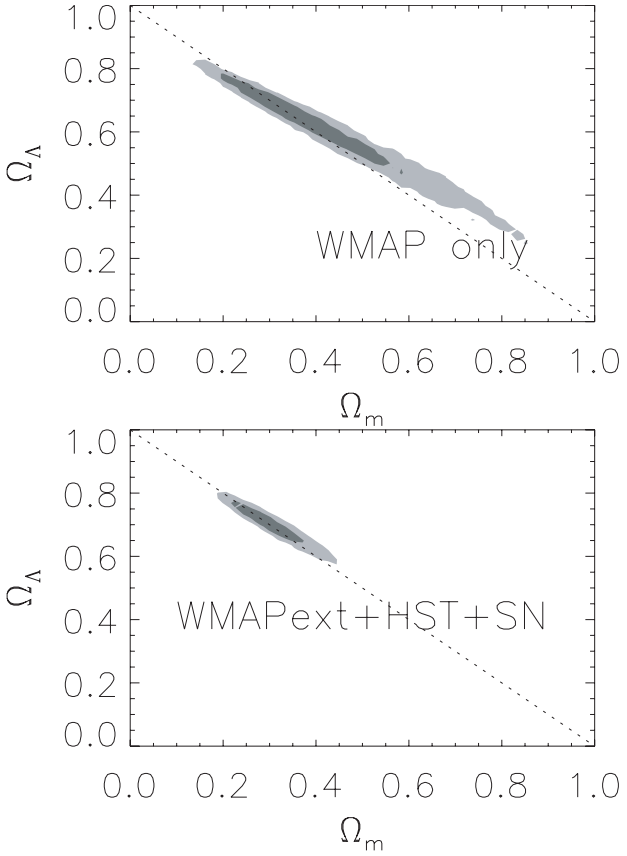

Fig. 19. Constraints on the geometry of the Universe shown in the $\Omega_M - \Omega_\Lambda$ plane. The figure shows the two dimensional likelihood surface for various combinations of data: upper plot WMAP data only and lower plot WMAP + CBI + ACBAR + HST Key Project + supernova data

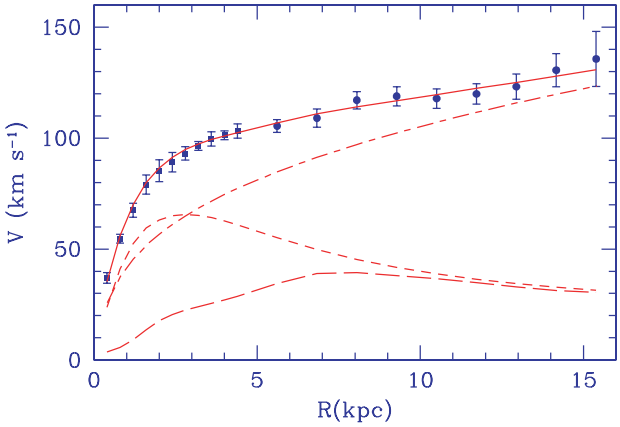

Fig. 20. M33 rotation curve (points) compared with the best fit dark matter halo model (*continuous line*). Also shown the halo contribution (*dashed-dotted line*), the stellar disk (*short dashed line*) and the gas contribution (*long dashed line*). From [31]

As an example the rotation curve of the nearby galaxy M33 is shown in Fig. 20 [31]. The rotation curve keeps rising out to the last measured point and implies a dark halo mass $\gtrsim 5 \times 10^{10}$ $M_\odot$. Results of the best fit to the mass distribution in M33 picture a dark halo which controls the gravitational potential from 3 kpc outward, with a matter density which decreases radially as $R^{-1.3}$. The density profile is consistent with the theoretical predictions for structure formation in hierarchical clustering cold dark matter models.

The nature of the CDM is unknown but the relic cold dark matter particles from the primordial Universe have to be electrical neutral, stable (or with $\tau \approx$ age of Universe) and massive. Therefore these Weakly Interaction Massive Particles (WIMP's) can not be particles which are known inside the framework of the Standard Model of particle physics.

The Standard Model of particle physics provides an excellent description of all physical processes that have been investigated up to now by experiments. Nevertheless most of the experts agree that physics beyond the standard model is probable. Supersymmetry (SUSY) is an ingredient that appears in many theories for physics beyond the standard model. In SUSY models with R-parity conservation the preferred candidate for a WIMP would be the lightest supersymmetric particle (LSP). This could be a neutralino, a sneutrino, a gravitino, an axino or even a particle not yet foreseen by theories. The most promising candidates for dark matter in most SUSY models is the neutralino.

7.1 SUSY dark matter

In the minimal supersymmetric extension of the Standard Model (MSSM) [12] the particle masses arise in much the same way as in the Standard Model. But the MSSM requires two Higgs doublets (H, $\bar{H}$) with opposite hypercharges in order to give masses to all the matter fermions, whereas one Higgs doublet would be sufficient in the Standard Model. The two Higgs doublets couple via an extra coupling called μ, and the ratio of the Higgs vacuum expectation values

$$\tan\beta = \frac{<\bar{H}>}{<H>} \tag{36}$$

is undetermined and is a free parameter in the MSSM.

For the the so-called constrained MSSM or CMSSM the supersymmetry-breaking masses of the different unseen scalar particles are assumed to have a universal value m_0 at some GUT input scale, and likewise the fermionic partners of the vector bosons are also assumed to have universal fermionic masses $m_{1/2}$ at the GUT scale.

A priori, the LSP might have been a sneutrino partner of one of the 3 light neutrinos, but this possibility has been excluded by a combination of the LEP neutrino counting and direct searches for cold dark matter. Thus,

the LSP is often thought to be the lightest neutralino χ of spin 1/2, which naturally has a relic density of interest to astrophysicists and cosmologists: $\Omega_\chi h^2 = \mathcal{O}(0.1)$ [13].

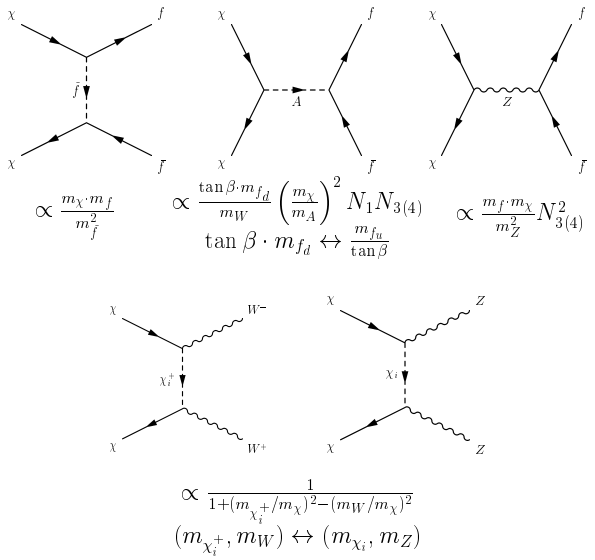

Fig. 21. Tree diagrams for Dark Matter annihilation. Note that the amplitudes of the top graphs are proportional to the mass of the final state fermion, while the Higgs exchange is proportional to $\tan\beta$ for d-type quarks and $1/\tan\beta$ for up-type quarks. This implies that light fermion final states can be neglected and at large $\tan\beta$ the bottom final states dominate. From [30]

The neutralinos are spin 1/2 Majorana particles, which can annihilate into fermion-antifermion pairs (see Fig. 21). The stable decay products are neutrinos, photons, protons, antiprotons, electrons and positrons. From these, the protons and electrons are drown in the many matter particles in the universe, but the others may be detectable.

The relic density can be calculated in the CMSSM using e.g. the package Micromegas, which is particularly suited for large $\tan\beta$, where the Higgs exchange and its loop corrected width are important [25]. The results are shown in Fig. 22 together with the constraints from electroweak precision data, as taken from [26].

Therefore using $\tan\beta = 50$ and $m_0 = 500\,Gev$, $m_{1/2} = 350\,GeV$, which specifies completely the CMSSM for $\mu > 0$ and $A_0 = 0$ the neutralino mass equals $0.4 m_{1/2} \approx 140$ GeV. These values are consistent with all known accelerator constraints and the relic density and, as will be shown below, describe the deficiencies of the galactic models very well.

Recently it was shown that Galactic Models testing all data on the abundance and spectra of matter particles and gamma spectra simultaneously show a deficiency in hard gamma rays and antiprotons and to a lesser extent in positrons [29].

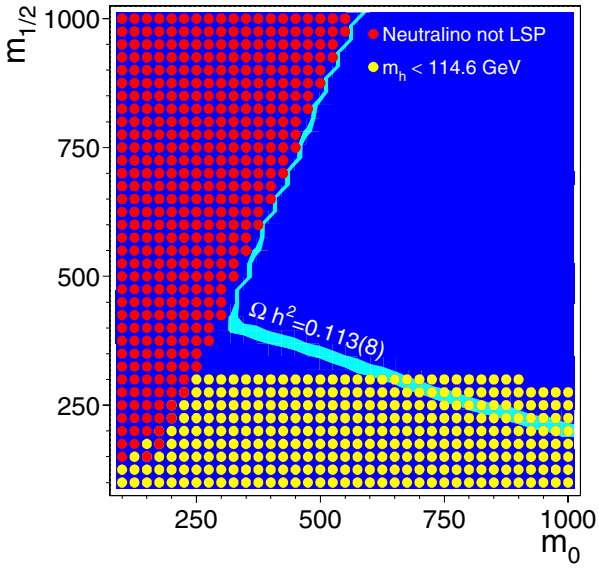

Fig. 22. The region of relic density allowed by the WMAP data. for $\tan\beta = 50$. The excluded regions, where the stau would be the LSP (red) or the Higgs mass too light (yellow), are also indicated. For lower values of $\tan\beta$ the allowed region rapidly shrinks. From [30]

The sources of charged and neutral cosmic rays are believed to be supernovae and their remnants, pulsars, stellar winds and binary systems. Observations of X-ray and γ-ray emissions from these objects reveal the acceleration of charged particles near them. Particles accelerated near the sources propagate tens of millions of years in the interstellar medium where they can loose or gain energy and produce secondary particles and γ-rays. The spallation of primary nuclei into secondary nuclei gives rise to rare isotopes. Nuclear interactions produce not only matter, but also antimatter, like antiprotons and positrons. The latter originate mainly from the decay of charged pions and kaons.

The detailed studies of cosmic rays tell us a lot about the production and propagation in the universe. The gammas can deliver information over intergalactic distances, while the charged particles propagate mainly on galactic distances. Secondary nuclei are produced in the galactic disk, from where they escape into the halo by diffusion and Galactic winds (convection).

A global fit to all this information allows one to build a model of our galaxy. The most complete and publicly available code for the production and propagation of particles in our galaxy is the Galprop code [27,28].

Figure 23 shows the composition of the primary and secondary nuclei, as calculated by Galprop in comparison with data. Clearly, the production of secondary nuclei is well described.

If one uses the recent measurements of the B/C ratio to further constrain the parameters of the Galprop model one predicts too few antiprotons, too few gammas

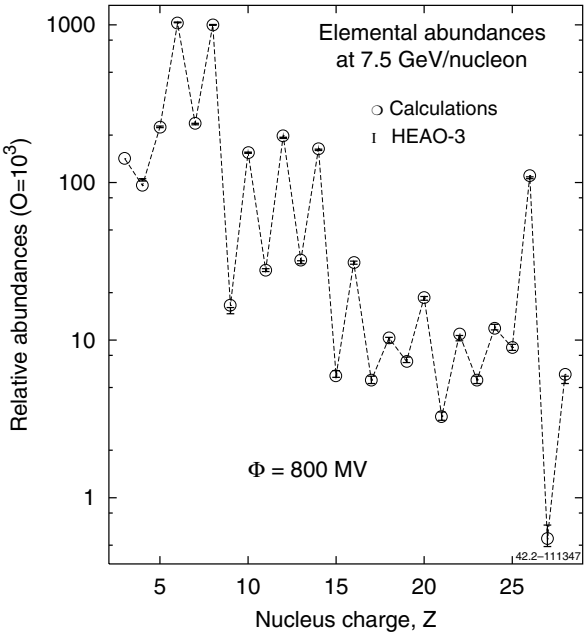

Fig. 23. Propagated abundances at 7.5 GeV/nucleon, as calculated by Galprop in comparison with data. From [29]

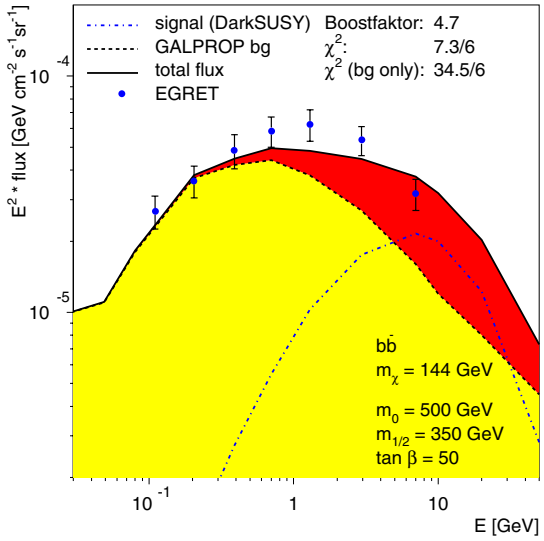

Fig. 24. Gamma ray spectrum with contributions from nuclear interactions (grey/yellow) and neutralino annihilation (dark/red). From [30]

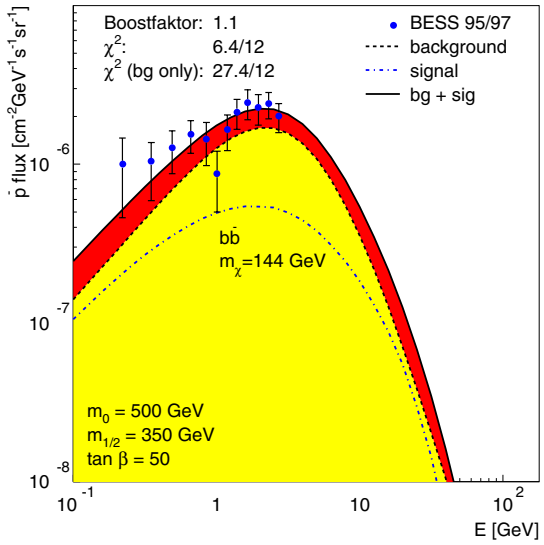

Fig. 25. Antiproton spectrum with contributions from nuclear interactions (grey/yellow) and neutralino annihilation (dark/red). From [30]

at high energies and a deficit in the positron/electron fraction compared to the data. The possible way out of the discrepancy was suggested by Strong and Moskalenko: a "fresh" local unprocessed component at low energies of primary nuclei, thus decreasing the B/C ratio and allowing for a smaller diffusion coefficient.

It can be shown that the neutralino annihilation in the Constrained Minimal Supersymmetric Model can perfectly take care of these deficiencies [30]. A global fit, including recent WMAP data and accelerator constraints, to the gamma rays (see Fig. 24), antiprotons (see Fig. 25) and positrons (see Fig. 26) fit both the *shape* AND *magnitude* of the spectra with boost factors close to unity [30].

The probability of the global fit improves by several orders of magnitude, if Dark Matter, as predicted by Supersymmetry, is taken into account for a usual NFW-type halo profile.

The inclusion of neutralino annihilation improves the fit considerably, as is obvious from the figures, where the Galprop background from nuclear interactions and the signal from neutralino annihilation are indicated separately. The $\chi^2/d.o.f.$ is reduced from 121/35 for the background only fit to 34/35 for the fit including neutralino annihilation. This corresponds to an increase in probability from 2.10^{-9} to 0.49.

7.2 Indirect detetction of dark matter

In order to detect dark matter one strategy is to look for relic annihilations in the galactic halo, which might produce detectable antiprotons or positrons in the cosmic rays (PAMELA [33] and AMS-02 Experiment [32]). Alternatively, one might look for annihilations in the core of our galaxy, which might produce detectable gamma rays (GLAST Experiment [34]). A third strategy is to look for annihilations inside the Sun or Earth, where the local density of relic particles is enhanced in a calculable way by scattering off matter, which causes them to lose energy and become gravitationally bound. The signature would then be energetic neutrinos that might produce detectable muons. Several underwater and ice experiments are underway or planned to look for this signature [36, 35].

As an example the AMS-02 experiment and its discovery potential will be described in more detail in the following.

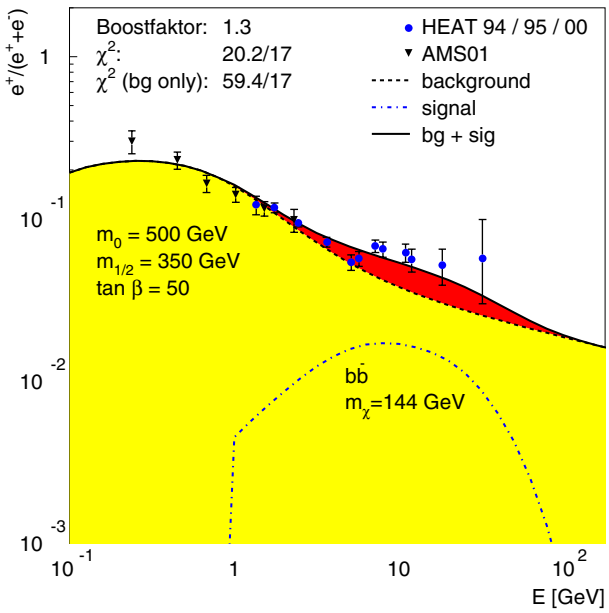

Fig. 26. Positron spectrum with contributions from nuclear interactions (grey/yellow) and neutralino annihilation (dark/red). From [30]

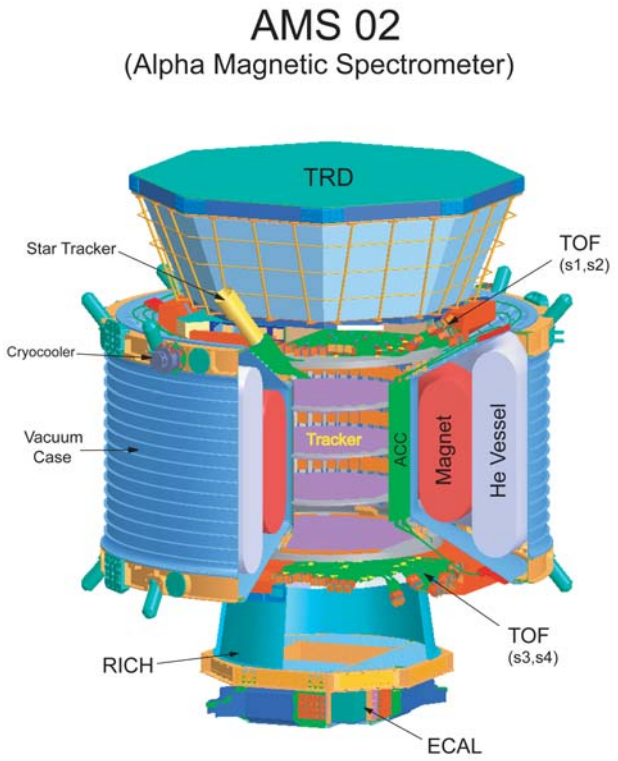

Fig. 27. Exploded view of the AMS-02 experiment

AMS-02 experiment

The AMS-02 experiment (see Fig. 27) will measure cosmic ray particle spectra on the ISS starting in summer 2007 for a period of 3 years. The main scientific focus is the search for anti matter and dark matter. With the AMS-01 [37] flight in 1998 on board of the Space Shuttle Discovery it was demonstrated for the first time that it is possible to operate a modern particle physics detector in space. The key element of the AMS-02 experiment is a superconducting magnet which generates in a cylindrical volume of 0.6 m^3 a magnetic field of 0.9 Tesla. Inside this volume a high precision double sided silicon strip detector measures the trajectories of charged particles at 8 planes with a precision of 8 micron per point in the coordinate perpendicular to the track. These precision measurements determine particle momentum and charge up to the TeV scale. The detector is completed on top by a transition radiation detector and on the bottom by a ring image cherenkov counter and an electromagnetic calorimeter for particle identification. The expected performance of AMS-02 should improve in all relevant aspects the previous measurements by several orders of magnitude.

The AMS experiment will allow direct searches for the various annihilation and decay products of WIMP's interacting with the galactic halo. These searches require high statistics precision measurements of positron (see Fig. 28) and anti proton spectra (see Fig. 29).

Cosmic radiation is dominated by protons. To measure positron spectra with high accuracy a very good proton-positron separation is required. The proton rejection has to reach a level of 10^6 up to particle energies of 300 GeV.

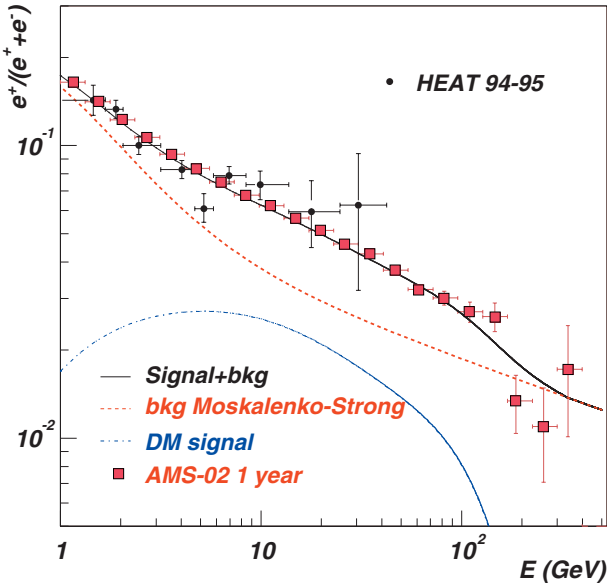

Fig. 28. Expected quality of AMS-02 data on the ratio $e^+/(e^+ + e^-)$ compared to the HEAT data together with a typical prediction in the framework of SUSY neutralino annihilation models

In AMS-02 this will be achieved by a combination of an electromagnetic calorimeter, proton rejection $10^3 - 10^4$, and a transition radiation detector (TRD) which should reach a proton rejection of $10^2 - 10^3$ depending on the particle momentum.

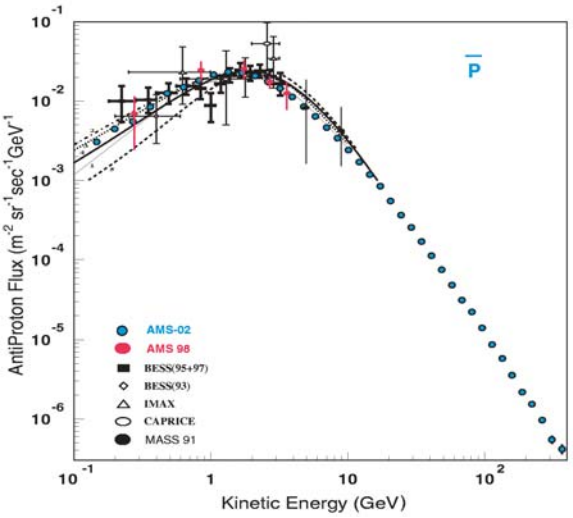

Fig. 29. AMS-02 will measure the antiproton spectrum with a few percent energy resolution up to hundreds of GeV

The AMS-02 measurements will also help to constrain the galactic halo models and hence allow to interpret a possible excess in the positron fraction. As an example in Fig. 30 the ratio of $^{10}Be/^{9}Be$ is shown. The lifetime of ^{10}Be is 1,5 million years compared with the stable isotope ^{9}Be and its abundance is one of the prime determinants of the halo size.

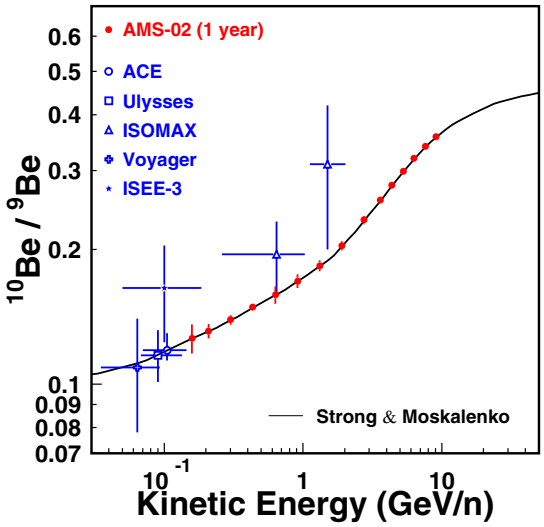

Fig. 30. AMS-02 will measure the ratio of the $^{10}Be/^{9}Be$ isotopes

In Fig. 31 the spectrum of the Boron over Carbon (B/C) ratio is displayed, which shows a characteristic depletion at low energies. Since Boron is a purely secondary produced nucleus, while Carbon is primarily produced, the depletion at low energy is a sensitive handle on the question of diffusive re-acceleration and solar modulation.

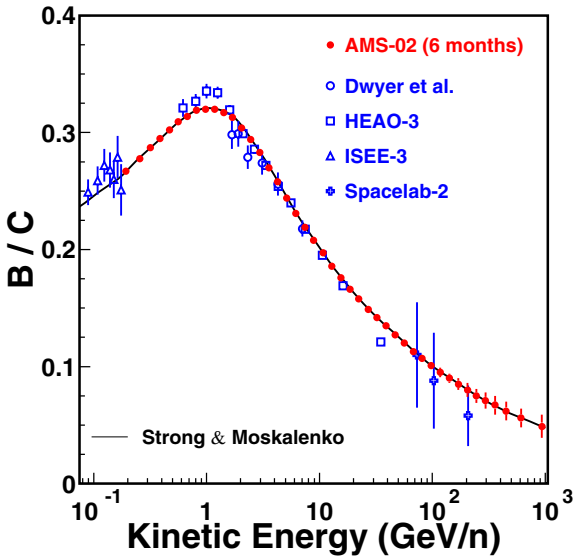

Fig. 31. The B/C ratio as example of secondary/primary nucleon as expected from the AMS-02 measurements compared with existing data sets

From PAMELA we can expect the first data in 2005 while GLAST and AMS-02 will hopefully start to produce physics results in 2007. The precision measurements of cosmic rays that we can expect from these experiments will open a new window to understand the nature of dark matter. Especially in combination with the SUSY search at LHC we have an extremely exciting period of particle and astroparticle physics ahead of us.

7.3 Direct detetction of dark matter

The most satisfactory way to look for supersymmetric relic particles is directly via their elastic scattering on nuclei in a low-background laboratory experiment. There are two types of scattering matrix elements, spin-independent - which are normally dominant for heavier nuclei, and spin-dependent - which could be interesting for lighter elements such as fluorine. The best experimental sensitivities so far are for spin-independent scattering.

A large variety of techniques (see Fig. 32) is used for the direct search for dark matter. The various approaches have different systematic errors which is extremely important in case of a positive signal.

The basic idea for all experiments is rather simple. The WIMP elastically scatter off a nucleus, the recoil energy spectrum of which is measured in the target. Due to the rotation of the earth around the sun with a speed of 30 km/s (15 km/s projected on to the sun's motion) and the rotation of the sun around the galactic center $v_0 = 230\ km/s$ (see Fig. 33) one expects an annual modulation of the signal at the 2% level if one assumes for the WIMP's an isothermal halo with no co-rotation.

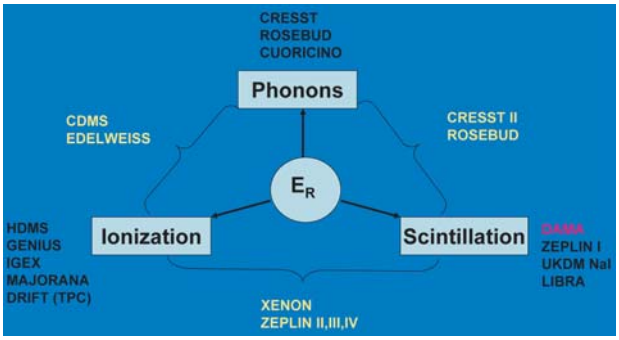

Fig. 32. The various techniques used for the search for WIMPS. From [38]

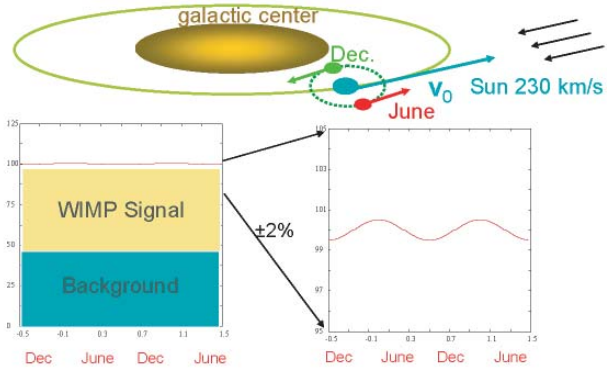

Fig. 33. Expected annual modulation of a WIMP signal. From [38]

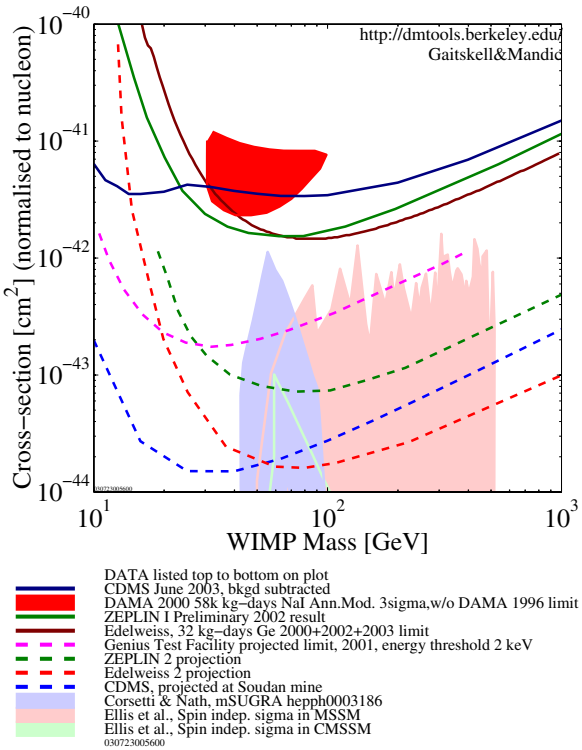

Fig. 34. Exclusion limits obtained from the listed experiments (*full lines*) together with the positive signal from DAMA [39] and the expected improvements in the near future (*dashed lines*)

All techniques have equally aggressive projections for future performance, but use different methods for improving the sensitivity (see Fig. 34). The current exclusion limits hardly touch the interesting SUSY parameter space while the next generation of experiments will cover a large part. The direct search for dark matter will become extremely interesting within the next few years.

A major point of understanding of these detectors is to keep in mind the amount of energy and the resulting signal heights we are dealing with:

- the kinetic energy of the recoiling nucleus is of few KeV
- the heat increased is of the order of 10^{-6} degrees,
- the power variation at the micro-watt level,
- the ionization collected charge is of few hundreds of electrons.

DAMA Experiment

The only experiment which has claimed already in 1996 a positive WIMP signal was the $\approx 100kg$ NaI(Tl) DAMA experiment using 4 annual cycles [39]. In the year 2000 a full substitution of the electronics and the DAQ took place. With the new data (see Fig. 35), published in summer 2003 [40], DAMA could show that the running conditions are stable at the $< 1\%$ level. The observed oscillation curve can be parametrized as

$$s(t) = A \cdot \cos[\omega(t - t_0)] \qquad (37)$$

where one expects that $t_0 = 152.5\ days$ (signal maximum in summer) and $T = 1.00\ year$. Using the cumulative 7 annual cycles exposure the DAMA collaboration finds: $A = (0.0200 \pm 0.0032)\ cpd/kg/KeV$, $t_0 = (140 \pm 22)\ days$ and $T = (1.00 \pm 0.01)\ years$. The $\chi^2/dof = 71/37$ and the probability for a fit with $A = 0$ is $P(A = 0) = 7 \cdot 10^{-4}$. The data therefore favor the presence of a modulated behavior with the proper features at the 6.3 σ confidence level. A deep investigation by the DAMA collaboration has shown no known sources of possible systematics and side processes able to mimic the signature.

For most of the experiments it will be difficult to prove or disprove the DAMA findings as their detector mass is too small to be sensitive to annual modulations and different to DAMA where the 100 kg NaI detector is fully sensitive to Spin dependent WIMP couplings the Ge- and Si-detectors are mostly sensitive to the Spin independent couplings. Only the GENIUS TF [41] experiment has a large enough mass to be able to confirm the DAMA results if the WIMP couplings are spin independent. One expects that GENIUS TF starts data taking early 2004.

8 Summary

The combination of the various cosmological observations presents strong evidence that the energy density of the

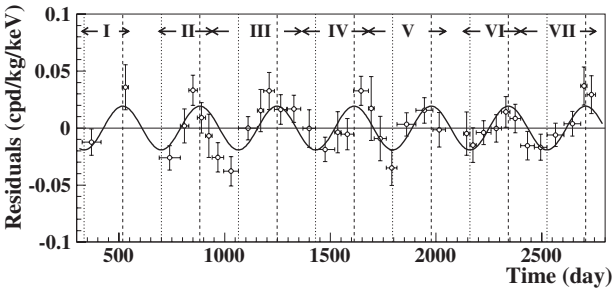

Fig. 35. Model independent residual rate for single hit events, in the $(2-6)$ keV energy intervals as a function of the time elapsed since January 1-st of the first year of data taking. The superimposed curves represent the co-sinusoidal functions behaviors expected for a WIMP signal with a period equal to 1 year and phase at 2nd June; the modulation amplitudes have been obtained by best fit. From [40]

Universe is dominated by an unexpected form of negative-pressure, the so called "dark" energy. It is also obvious that the matter density of the Universe is dominated by cold dark matter.

In the near future we expect from the ongoing WMAP program and from SDSS that we are able to confirm that our cosmological model describes nature and that we are able to perform precision measurements of the cosmological parameters. We have to understand the nature of Dark matter and Dark energy and their implications for fundamental physics.

The Standard Model of particle physics is the basis of any description of the physics of the early Universe. Its possible extensions, for example in the SUSY framework, may provide the answers to many of the outstanding issues in cosmology. What is the nature of dark matter and dark energy ? What is the origin of matter in the Universe ? Continued progress in understanding these issues will involve a complex interplay between particle physics and cosmology, involving experiments at new accelerators such as the LHC.

A new generation of space experiments for the precision measurements of cosmic rays like PAMELA, GLAST and AMS will open a new window to understand the nature of dark matter. DAMA has claimed evidence with 6.3 σ C.L. to have observed the expected annual modulation for a WIMP signal. A variety of direct WIMP search experiments have shown evidence that they will reach within the next few years a sensitivity necessary to discover dark matter as predicted by SUSY models.

References

1. G. Börner: *The Early Universe*, Springer, Berlin 2003;
   L. Bergström and A. Goobar: *Cosmology and Particle Astrophysics*, John Wiley & Sons Ltd, England, 1999
   W.H. Kinney: "Cosmology, Inflation, and the Physics of Nothing", astro-ph/0301448
2. D.N. Spergel et al. (WMAP Collaboration): astro-ph/0302209
3. For an excellent introduction into CMB physics see Wayne Hu's WWW-page:
   http://background.uchicago.edu/~whu/
   W. Hu.: *CMB temperature and polarization anisotropy fundamentals*. Annals of Physics, **303**, 203–225, Jan. 2003
   A. Kosowsky: "The Cosmic Microwave Background", astro-ph/0102402 v1, Feb. 2001. Lectures given at the Italian Society of Gravitational Physics Summer School "Relativistic Cosmology: Theory and Observation" in Como, Italy (May 2000)
4. Max Tegmark: http://www.hep.upenn.edu/~max/
5. G.F.Smoot et al. (COBE Collaboration): Astrophys. J. **360**, 685 (1990)
6. The results of the first year of operation of the WMAP satellite can be found on the Web:
   http://map.gsfc.nasa.gov/m_mm/pub_papers/firstyear.html
7. C.L. Bennett, et al. (WMAP Collaboration): astro-ph/0302207
8. L. Verde et al. (WMAP Collaboration): astro-ph/0302218
9. Pearson et al. (CBI Collaboration): astro-ph/0205388
10. Kuo et al. (ACBAR Collaboration): astro-ph/0212289
11. Freedman et al. (HST Key Project): P.B. 2001, ApJ **553**, 47
12. H.E. Haber and G.L. Kane: Phys. Rep. **117**, 75 (1985)
13. J. Ellis, J.S. Hagelin, D.V. Nanopoulos, K.A. Olive, and M. Srednicki: Nucl. Phys. B **238**, 453 (1984)
14. M. Colless et al. (2dF Collaboration): astro-ph/0306581 v1, Jun. 2003
15. O. Elgaroy and O.Lahav: astro-ph/0303089 v3, May 2003
16. O. Elgaroy et al.: Phys. Rev. Letters **89**, (2002)
17. K. Abazajian et al. (SDSS collaboration): 2003, ArXiv Astophysics e-prints, 5492
18. M. Tegmark et al.: astro-ph/0310571
19. T.P. Walker, G. Steigman, D.N. Schramm, K.A. Olive, and K. Kang: Ap. J. **376** 51 (1991); S. Sarkar: Rep. Prog. Phys. **59**, 1493 (1996); K.A. Olive, G. Steigman, and T.P. Walker: Phys. Rep. **333**, 389 (2000); B.D. Fields, and S. Sarkar: Phys. Rev. D **66** (2002) 010001.
20. R.H. Cyburt, B.D. Fields, and K.A. Olive: astro-ph/0302431
21. R.H. Cyburt, B.D. Fields and K.A. Olive: New Astron. **6**, 215 (1996) [arXiv:astro-ph/0102179]
22. J.L. Tonry et al. (HZT Collaboration): astro-ph/0305008 v1, May 2003
23. A.G. Riess et al.: AJ, **116**, 1009 (1998)
24. S. Perlmutter et al.: ApJ, **517**, 565 (1999)
25. G. Bélanger, F. Boudjema, A. Pukhov, and A. Semenov: "micrOMEGAs: Recent developments", arXiv:hep-ph/0210327 and
   http://wwwlap.in2p3.fr/lapth/micromegas
26. W. de Boer and C. Sander: "Global Electroweak Fits and Gauge Coupling Unification", arXiv:hep-ph/0307049
27. A.W. Strong and I.V. Moskalenko: Astrophys. J. **509**, 212 (1998)
28. I.V. Moskalenko and A.W. Strong: Astrophys. J. **493**, 694 (1998)
29. A.W. Strong, I.V. Moskalenko, S.G. Mashnik, and J.F. Ormes: Astrophys. J. **586**, 1050 (2003)

30. W. de Boer, M. Herold, C. Sander, and V. Zhukov: "Indirect Evidence for Neutralinos as Dark Matter", hep-ph/0312037, Presented at International Europhysics Conference on High-Energy Physics (HEP 2003), Aachen, Germany, 17–23 Jul 2003
31. E.Corbelli and P. Salucci: astro-ph/9909252 v1, Sep. 1999
32. AMS Collaboration: home page: http: hpl3tri1.cern.ch/AMS/
33. PAMELA Collaboration: home page: http: wizard.roma2.infn.it/pamela/
34. Proposal for the Gamma-ray Large Area Space Telescope, SLAC-R-522 (1998) GLAST Proposal to NASA A0-99-055-03 (1999)
35. U.F. Katz: "Status of the ANTARES Project", astro-ph/0310736
36. F. Halzen: "High-Energy Neutrino Astronomy: From AMANDA to IceCube", astro-ph/0311004
37. M. Aguilar et al. (AMS-01 Collaboration): Physics Reports **366/6**, 331-404 (Aug. 2002),
38. L. Baudis: "Experimental searches of dark matter", talk presented at CAPP 2003, CERN, 12.-17. June 2003, http://wwwth.cern.ch/capp2003/
39. R. Bernabei et al. (DAMA collaboration): Phys. Letter B **389**, 757 (1996)
40. R. Bernabei et al. (DAMA collaboration): Riv. N. Cim 26 n.1. 1–73 (2003)
41. H.V. Klapdor-Kleingrothaus, L. Baudis, A. Dietz, G. Heusser, I. Krivosheina, B. Majorovits, and H. Strecker: NIM A **481/1-3**, 149–159 (2002)